Pit nucleation on as-cast aluminiuim alloy AW-5083 in 0.01M NaCl

Dolic, Natalija; Malina, Jadranka; Begić Hadžipašić, Anita

Source / Izvornik: **Journal of Mining and Metallurgy, Section B: Metallurgy, 2011, 47, 79 - 87**

Journal article, Published version
Rad u časopisu, Objavljena verzija rada (izdavačev PDF)

https://doi.org/10.2298/JMMB1101079D

Permanent link / Trajna poveznica: https://urn.nsk.hr/urn:nbn:hr:115:339642

J. Min. Metall. Sect. B-Metall. 47 (1) B (2011) 79 - 87

Journal of Mining and Metallurgy

PIT NUCLEATION ON AS-CAST ALUMINIUIM ALLOY AW-5083 IN 0.01M NaCl

N. Dolić#, J. Malina and A. Begić Hadžipašić

University of Zagreb Faculty of Metallurgy, Aleja narodnih heroja 3, 44103 Sisak, Croatia

(Received 07 December 2010; accepted 20 December 2010)

Abstract

The use of aluminium alloys in a wide range of technical applications is related mostly to the two facts: they facilitate weight saving of final products (if compared to the steel) and they are prone to spontaneous passivity due to the coherent surface oxide layer which impedes further reaction of aluminium with the environment.

Among the commercial Al alloys, EN AW-5083 alloy is a representative non-heat treatable Al-Mg based alloy which possesses many interesting characteristics as a structural material, such as low price, moderately high strength, high formability in conjunction with superplasticity and good corrosion resistance in marine atmospheres. Aiming to enhance the knowledge of possible interactions of studied alloy EN AW-5083 in as-cast condition with chloride media, electrochemical measurements were used to follow the pitting behaviour in 0.01 M NaCl. The results of tests have shown that susceptibility of alloy to pitting corrosion is strongly influenced by the microstructural constituents of the alloy in as-cast condition.

Key words: aluminium alloy EN AW-5083, as–cast microstructure, chloride medium, pitting

1. Introduction

New antipollution and energy-saving laws impose a reduction in fuel consumption for vehicles of the automotive industry. This reduction may be obtained through the lightening of vehicles by making car-bodies out of aluminium alloys instead of steel or by making some components out of light alloys as aluminium or magnesium alloys [1, 2]. However, using aluminium to replace steel has two major disadvantages. The first disadvantage is that aluminum alloys cannot meet the maximum yield strengths required

Corresponding author: ndolic@simet.hr

DOI:10.2298/JMMB1101079D

in certain building applications where only high-strength, low-alloy steels meet high strength requirements. The second disadvantage is that aluminum costs roughly five times more than steel [3].

Anyway, the 5xxx series aluminium alloys are resistant to a wide range of chemical and food products, making them especially useful in these industries [4]. Furthermore, aluminium magnesium casting alloys are used for high strength foil, dump track bodies, petrol tanks, pressure cryogenic vessels, marine structures and fittings, automotive trim and architectural components. In shipbuilding they are commonly used due to low density, good mechanical properties and very good anticorrosion properties in general conditions and marine atmospheres. However, in environments where chloride ions may have a contact with Al alloys, pitting nucleation starts and such local corrosion mechanisms can result in very serious damages [5, 6]. In order to enhance the knowledge of possible interactions of studied alloy EN AW-5083 in as-cast condition with chloride media, in this study the electrochemical methods were used to follow the pitting behaviour in 0.01 M NaCl.

2. Experimental

2.1. Material

Specimens for chemical, microstructural and electrochemical investigations were prepared from the commercial ingot (10 tons in weight, 1680x520x4809 mm in size) of AlMg alloy produced by semicontinuous vertical direct-chill casting process in TLM - Šibenik, Croatia. Before casting, the melt was refined with an argone and chlorine mixture in an Alpur unit. For grain refinement, the Al-Ti5-B1 master alloy was used in an average amount of 1.9 kg/t melt. Therefore the small bars of the alloy were added to the casting furnace, while Al-Ti5-B1 wire was introduced in a launder positioned in front of the Alpur unit [7]. Chemical composition was obtained by optical emission spectrometry.

2.2 Electrochemical testing

A three-electrode system including a working electrode, an auxiliary electrode and a reference electrode was used for the electrochemical measurements. The auxiliary electrode is a platinum mesh and the reference electrode is a saturated calomel electrode (SCE) with a fine Luggin capillary positioned close to the working electrode surface in order to minimize ohmic potential drop. The working electrodes were made of cylinder specimens with an round surface of 2.83 cm^2. They were embedded in glass holder using epoxy resin. The electrolyte was 0.01 mol/L NaCl.

Each sample was successively polished using SiC emery papers from 400 to 800 grades on the test face, then rinsed with distilled water, degreased with ethanol, and dried in air. Before each run, the working electrode was immersed in the cleaning solution 0.1 M NaOH for 1 min at 40 °C.

All the potentials reported here were measured against the saturated calomel electrode. To obtain the parameters of local corrosion, polarization curves were performed by polarizing the working

electrode in the anodic direction starting from -1.5 V to -0.2 V vs SCE and back at a scan rate of 5 mV/s. All the potentiodynamic scanning experiments were performed by Potentiostat/Galvanostat (Princeton Applied Research) PARSTAT 2273. Each experiment was repeated at least three times to check the reproducibility.The experiments were carried out at room temperature (293K).

2.3. Microstructural analysis

The microstructure of sectioned AlMg specimens was examined using optical microscopy before and after the electrochemically induced pitting. Metallographic preparation involved methods of standard surface preparation [8].

Second phase particles in Al-rich matrix were analysed by using SEM („TESCAN VEGA TS5136LS“) equipped with EDS system („Oxford Instruments“).

3. Results and discussion

3.1. Chemical analysis

The composition of AlMg alloy in mass percentage is listed in Table 1. According to wrought aluminium alloys designation system, it belongs to group 5xxx, which includes magnesium as the major alloying element (up to 5.6 %). Mg is used for solid solution hardening, while manganese, chromium, titanium, vanadium, beryllium may be added to the alloys of 5xxx series as minor alloying elements. In concordance to European Norms, the alloy is known as EN AW–5083 with chemical symbol EN AW-AlMg4.5Mn0.7.

3.2. Electrochemical testing

In order to follow the nucleation of pits on the surface of AlMg alloy in 0.01 M NaCl, the breakdown potential should be obtained from the experimental polarization curves. Therefore potentiodynamic polarization measurements were carried out and Fig. 1 shows the experimental plot with parameters of local corrosion. The potential is scanned in the anodic direction until localized corrosion initiates as indicated by a large increase in the current. The potential at this point is denoted as E_{bd}, the breakdown potential above which pits are nucleated. If scan is reversed, the anodic current decreases until it becomes zero and changes the polarity. The potential at this point is defined as E_{rp}, the repassivation potential below which pits repassivate. Thus, the higher the value of E_{bd}, the more resistant is the alloy to the initiation of localized attack. The higher E_{rp}, the more easily the alloy can repassivate. At potentials between $E_{bd\ and}$ E_{rp}, pits that have initiated can propagate. Based on this argument, one would favor an alloy that had both a high E_{bd} and a high E_{rp}. Such an alloy is characterized by narrow hysteresis loop ($E_{hys} = E_{bd} - E_{rp}$), Fig. 1.

Table 1. Chemical composition (mas. %) of AlMg alloy EN AW-5083

Element composition, mas. %									
Mg	Mn	Si	Fe	Cr	Cu	Zn	Ti	Be	Na
4.13	0.45	0.12	0.36	0.1	0.006	0.007	0.027	0.0036	0.0016

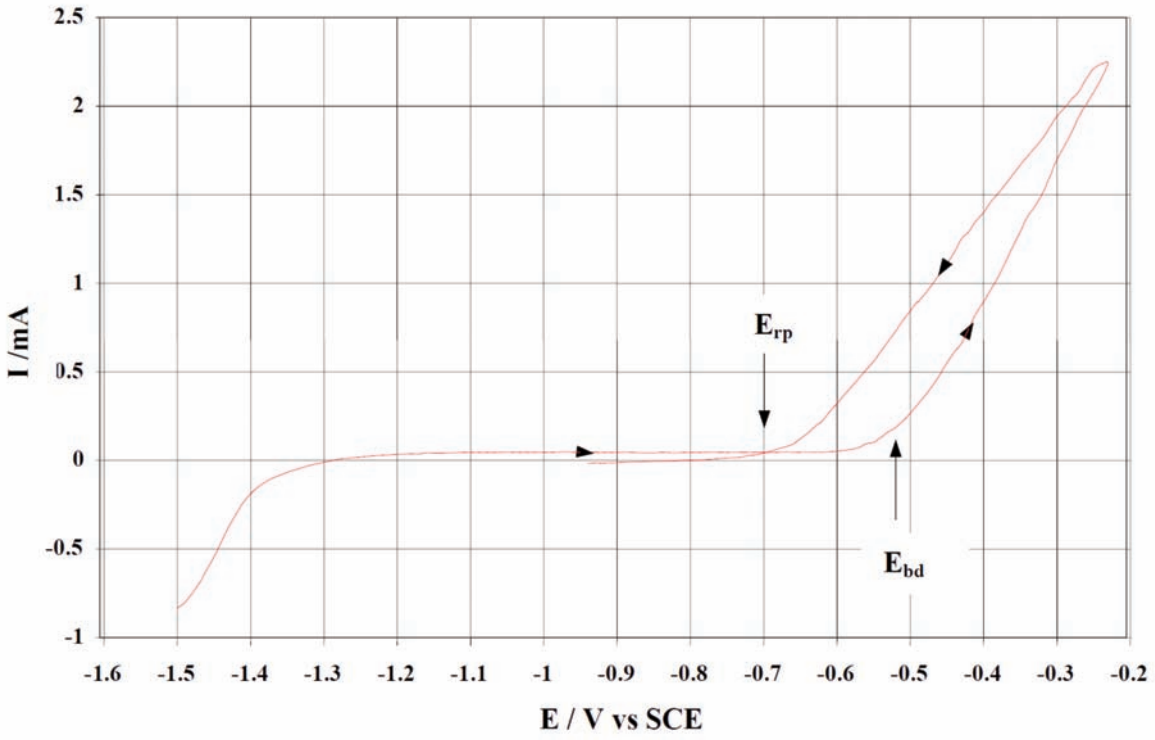

Fig. 1. Representative cyclic voltammogram for AlMg alloy EN AW-5083 in 0.01 M NaCl

The values of associated electrochemical parameters such as a corrosion potential (E_{corr}), breakdown potential (E_{bd}) and repassivation potential (E_{rp}) were obtained from the cyclic polarization curves and average values are listed in Table 2.

For the AlMg alloy examined, the potential range from -686 mV to -510 mV is characterized by metastabile equilibrium at the interface alloy/electrolyte, i.e. some pits are repassivating and some are deepening. In order to make these changes visible, optical microscopy was used to follow the surface changes in 0.01M NaCl at different time intervals (5, 10, 20, 40, 60 and 120 min) while applying the potential slightly nobler than E_{bd} (E = -0.500V).

Table 2. Electrochemical parameters related to pitting behaviour of AlMg alloy EN AW-5083

AlMg alloy	E_{corr}, mV	E_{bd}, mV	E_{rp}, mV	E_{hys}, mV
EN AW-5083	-902	-510	-686	176

3.3. Microstructural analyses

Metallographic studies were made at stages throughout the corrosion test and these are discussed and related to the pitting process. The micrographs on Fig. 2 to Fig. 5 illustrate the presence of local galvanic couples heterogeneously dispersed on the surface of AlMg alloy.

Different positions in Fig. 2 where

analyzed by SEM/EDS so that chemical compositions of intermetallic phases (detail 1, detail 2) and matrix could be revealed, Fig. 3.

The relative values obtained suggest that compact light particles in the center area of marked detail are rich in iron and manganese if compared to aluminium matrix (detail 3). According to the literature [5, 6, 9, 10] they could be identified as Al_6 (Fe, Mn). Besides, different types of phases are particles shown in detail 2. Such dark, chinese script - like particles rich in Mg and Si are representative of the Mg_2Si phase [12-14].

Front the above it is obvious that two main types of microconstituents in AlMg alloy studied are Fe-rich and Mg-rich phases. They contribute to the heterogeneity of the surface, so that local micro-galvanic couples are formed if the metal is in contacts with the electrolyte. Namely, it is quoted in the literature [12] that Al_6 (Fe, Mn) phase is more noble than aluminium matrix, while the corrosion potential of Mg_2Si particles is almost the same or slightly lower than the one of Al [15].

The exposure of such alloy to the aggressive chloride medium results in the surface morphology changes, depending on

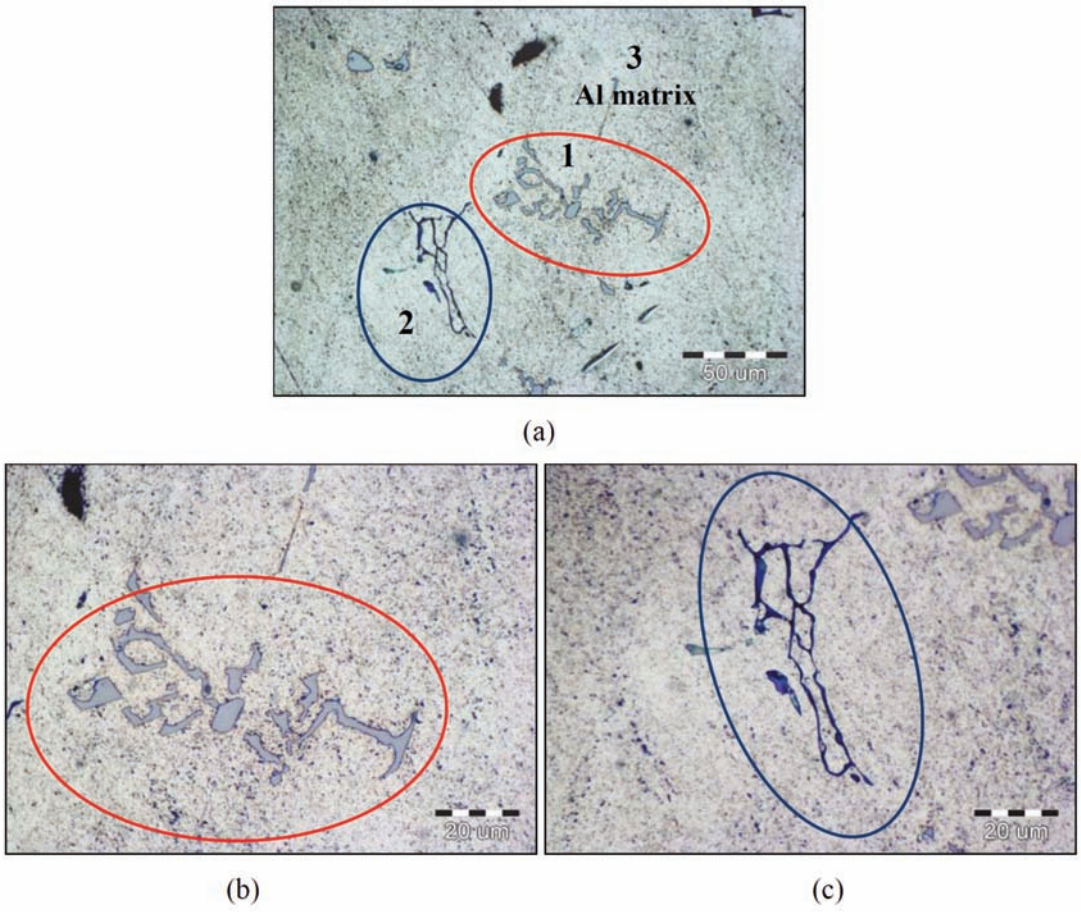

Fig. 2. Different intermetallic phases (a) detected by optical microscopy on the surface of AlMg alloy EN AW-5083 before the contact with 0.01 M NaCl: (b) detail 1; (c) detail 2

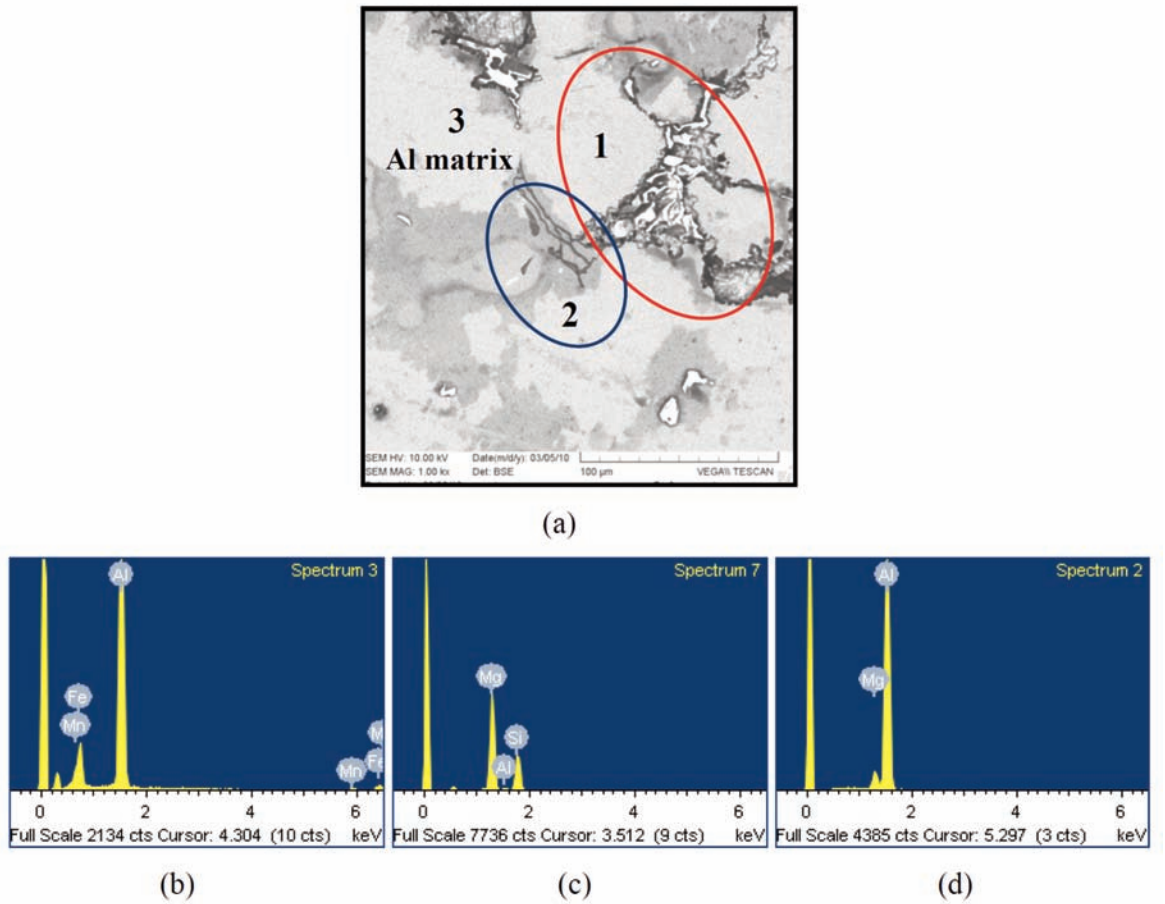

Spectrum	Mg		Al		Si		Mn		Fe	
	mas. %	at. %	mas. %	at. %	mas. %	at. %	mas. %	at. %	mas. %	at. %
Detail 1	4.77	5.27	95.23	94.73	-	-	-	-	-	-
Detail 2	-	-	57.01	73.27	-	-	3.93	2.48	39.05	24.25
Al-rich matrix	59.35	62.75	1.37	1.3	39.28	35.95	-	-	-	-

Fig. 3. SEM micrography (BSE mode) of intermetallic phases marked on the surface of AlMg alloy EN AW-5083(a) and their EDS spectrum/chemical composition after the polarization at -0.500V vs SCE for 120 min, (b) detail 1: Al_6(Fe, Mn), (c) detail 2: Mg_2Si, (d) Al-rich matrix

the anodic potential imposed to the specimen as well as on the contact time with the 0.01 M NaCl. The results in Fig. 4 show the extent of pitting corrosion started at anodic potential slightly higher than E_{bd}.

It has to be noted that even after short period of contact (10 minutes), the corrosion process is clearly visible in the neighborhood of the particles containing iron: the metallic matrix changed the color into more yellow nuance.

Further exposure to 0.01 M NaCl within

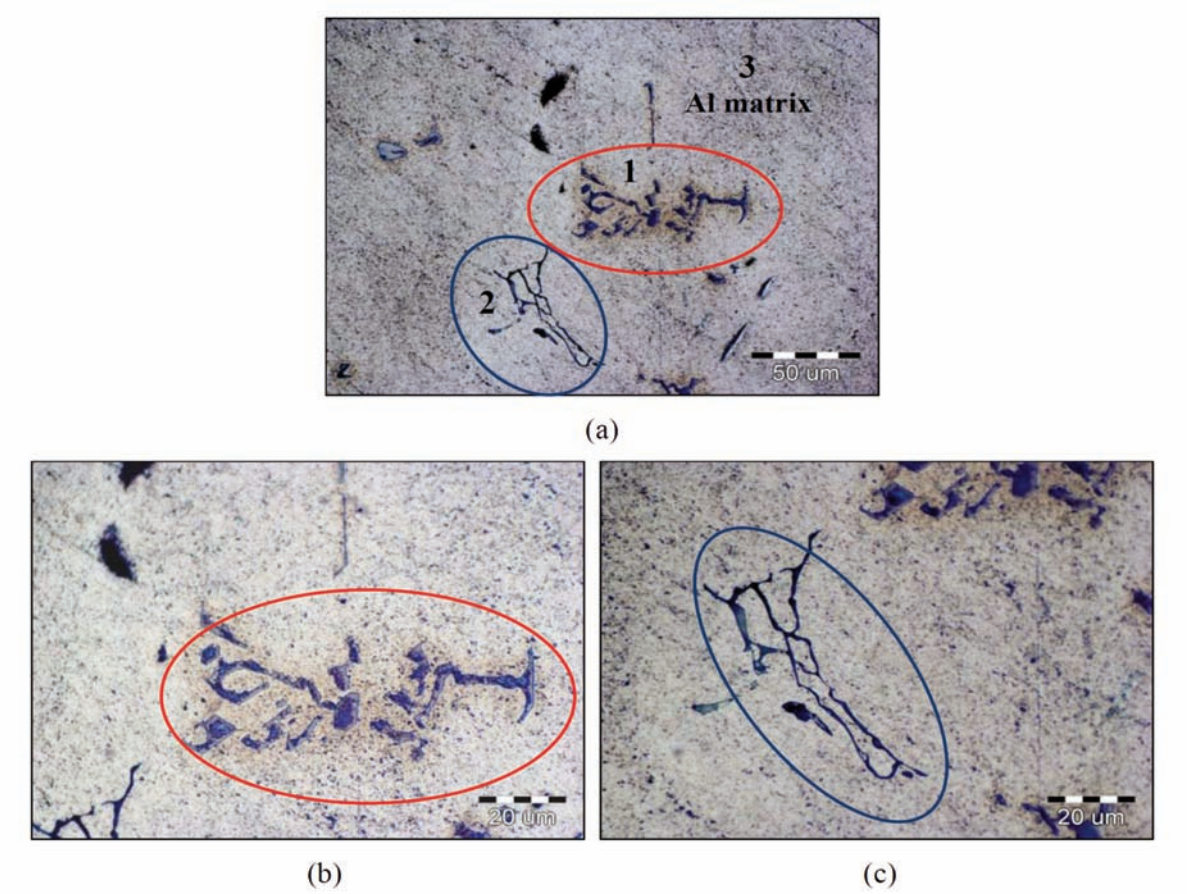

Fig. 4. Different intermetallic phases (a) detected by optical micrography on the surface of AlMg alloy EN AW-5083 after the polarization at -0.500 V vs SCE for 10 min:(b) start of local corrosion at detail 1; (c) detail 2

the 120 minutes resulted in the intensive pitting process around the Al_6 (Fe, Mn) particles, as it can be seen in Fig. 5.

Fig. 5 shows that main corrosion attack is focused on the metallic matrix surrounding the Al-Fe intermetallic particles while they stay intact (compare to Fig. 3a). The pits nucleate and propagate due to the local corrosion processes in the surface galvanic couples between more noble Al-Fe phases and active Al-rich matrix [12].

Basic anodic process is the corrosion of aluminium according to the equation:

$$Al \rightarrow Al^{3+} + 3e^- \quad ...(1)$$

This reaction is also the consequence of the "weak" oxide layer in that zone [13]. Simultaneously, the reduction of oxygen on intermetallic Al-Fe particles can be presented by equation (2):

$$O_2 + 2H_2O + 4e^- \rightarrow 4OH^- \quad ...(2)$$

OH^- - ions in solution cause the local pH increase which results in the dissolution of both, the oxide layer firstly (around the particles) and of the metallic matrix subsequently [15, 16]. According [12],

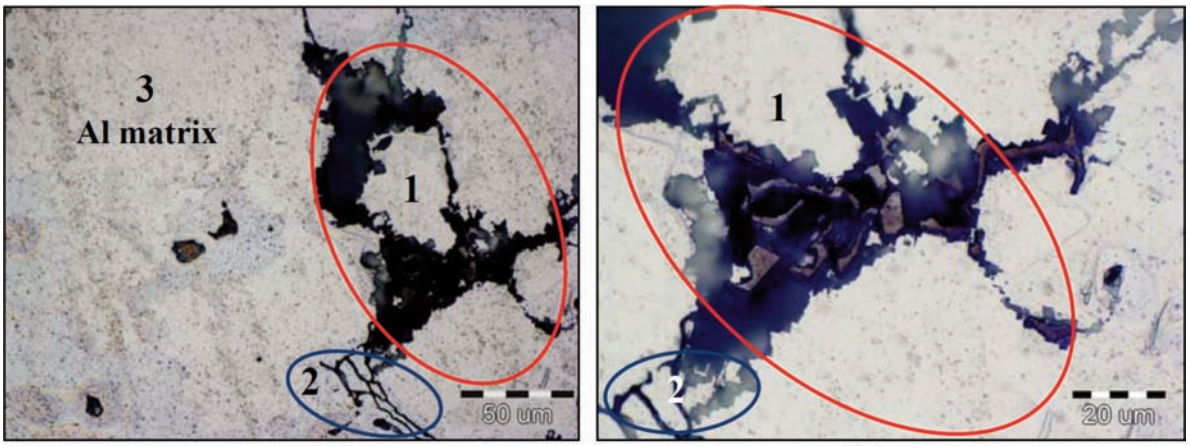

Fig. 5. Different intermetallic phases (a) detected by optical microscope on the surface of AlMg alloy EN AW-5083 after the polarization at -0.500V vs SCE for 120 min: (b) pit nucleated and grown at detail 1

statistical analysis of numerous pits nucleated in the vicinity of Al-Fe phases has shown that the eventual presence of Si and Cr in the intermetallic phases has the same influence on the pitting initiation as the presence of $Al_6(Fe, Mn)$.

In contrast to the expectations, Mg_2Si phases, although of anodic character if compared to Al, did not changed their morphology or influenced the matrix dissolution, as it can be seen in Fig. 4 and Fig. 5. The explanation is given in which both, the chemical and electrochemical reaction of Mg_2Si particles in water solutions [12, 14] are responsible for such a peculiar behavior described by the following equations:

$$Mg_2Si + 4\,H_2O \rightarrow 2Mg(OH)_2 + SiH_4 \quad ...(3)$$

$$SiH_4 + mH_2O \rightarrow SiO_2 \cdot nH_2O + H_2\uparrow \quad ...(4)$$

$$Mg_2Si + 2H_2O \rightarrow 2Mg^{2+} + SiO_2 + 4H^+ + 8e^- \quad ...(5)$$

It is obvious that Mg_2Si phase undergoes the hydrolysis step resulting in $Mg(OH)_2$ deposits at first, while SiO_2 is formed at the surface by electrochemical dissolution of Mg_2Si particles. They both, $Mg(OH)_2$ and SiO_2 are acting as a diffusion barrier and protect the particles of Mg_2Si from further dissolution.

Therefore, the chinese script-like particles identified in Fig. 2 to Fig. 5 have the same, unchanged morphology before and after electrochemical treatment and no dominant influence on pitting behavior of EN AW-5083 alloy in 0.01 M NaCl. However, their change in the number, shape and distribution, which depends on homogenization [17, 18], could influence the local corrosion and should be investigated in further studies.

4. Conclusion

On the basis of electrochemical, metallographic and SEM analyses of AlMg alloy EN AW-5083 in the as-cast condition it was revealed that surface passive film

formed spontaneously in air loses its protective character when alloy is anodically polarized in contact with solution of 0.01M NaCl. At a scanning rate of 5 mV/s, the breakdown of a passive layer starts at the breakdown potential E_{bd} = – 0.510 V vs SCE.

Pitting susceptibility can be related to the presence (in Al-rich matrix) of different intermetallic phases which exposed on the surface of alloy create a great number of local corrosion cells. Phases Al_6(Fe, Mn) are acting like cathodes and they induce anodic dissolution of surrounding matrix where pits nucleate.

It was shown that dissolution of Al is localized on the phase boundary between Al_6(Fe, Mn) particles and metallic matrix, with pit density higher on the surfaces with more intermetallic phases present.

Aknowledgment

This work was supported by the Ministry of Science, Education and Sports of the Republic of Croatia, within the project 124-1241565-1524 »Environmentally assisted degradation of metals and adsorption on waste C-materials».

References

[1] G. Sierra, P. Peyre, F. Deschaux-Beaume, D. Stuart, G. Fras, Mat. Sci. Eng. A, 447 (2007) 197.

[2] J.H. Driver, O. Engler, Design of Aluminum Rolling Processes for Foil, Sheet, Plate,Ch. 4 in Handbook of Metallurgical Process Design (L. Xie, K. Funatani, G.E. Totten, eds.), CRC Press, NY, 2004, p.69.

[3] tc.engr.wisc.edu/uer/uer99/author1/content.html.

[4] C. Zhou, X. Yang, G. Luan, Scripta Materialia, 53 (2005) 1187.

[5] Z. Szklarska-Smialowska, Corros. Sci., 41 (1999) 1743.

[6] M. Bethencourt, F.J. Botana, J.J. Calvino, M. Marcos, J. Pérez, M.A. Rodriguez, Mater. Sci. Forum, 298-292 (1998) 567.

[7] N. Dolić, A. Markotić, F. Unkić, Metall. Mater. Trans. B, 38B (2007) 491.

[8] N. Dolić, Ph. D. Thesis, University of Zagreb Faculty of Metallurgy, Sisak, 2010.

[9] A. Aballe, M. Bethencourt, F.J. Botana, M.J. Cano, M. Marcos, 43 (2001) 1657.

[10] E.V. Koroleva, G.E. Thompson, G. Hollrigl, M. Bloeck, Corros. Sci., 41 (1999) 1475.

[11] A. Johansen, Ph. D. Thesis, The Norwegian University of Science and Technology, Trondheim, 2000.

[12] K.A. Yasakau, M.L. Zheludkevich, S.V. Lamaka, M.G.S. Ferreira, Electrochim. Acta, 52 (2007) 7651.

[13] M. Czechowski, J. Mater. Process. Technol., 164-165 (2005) 1001.

[14] G. Lucadamo, N.Y.C. Yang, C. San Marchi, E.J. Lavernia, Mater. Sci. Eng. A, 430 (2006) 230.

[15] K. Mizuno, A. Nylund, I. Olefjord, Corros. Sci. , 43 (2001) 381.

[16] M.A. Arenas, M. Bethencourt, F.J. Botana, J. de Damborenea, M. Marcos, Corros. Sci., 43 (2001) 157.

[17] X. Fang, M. Song, K. Li, Y. Du, J. Min. Metall. Sect. B., 46 (2010) 171.

[18] R. Prokić-Cvetković S. Kastelec-Macura, A. Milosavljević, O. Popović, M. Burzić, J. Min. Metall. Sect. B., 46 (2010) 193.